Active and fossil mantle flows in the western Alpine region unravelled by seismic anisotropy analysis and high-resolution *P* wave tomography

Simone Salimbeni[a,*], Marco G. Malusà[b,*], Liang Zhao[c,d], Stéphane Guillot[e], Silvia Pondrelli[a], Lucia Margheriti[f], Anne Paul[e], Stefano Solarino[g], Coralie Aubert[e], Thierry Dumont[e], Stéphane Schwartz[e], Qingchen Wang[c], Xiaobing Xu[c], Tianyu Zheng[c], Rixiang Zhu[c]

[a] *Istituto Nazionale di Geofisica e Vulcanologia, Sez. Bologna, Bologna, Italy*
[b] *Department of Earth and Environmental Sciences, University of Milano-Bicocca, Milan, Italy*
[c] *State Key Laboratory of Lithospheric Evolution, Institute of Geology and Geophysics, Chinese Academy of Sciences, Beijing, China*
[d] *CAS Center for Excellence in Tibetan Plateau Earth Sciences, Beijing, China*
[e] *Univ. Grenoble Alpes, Univ. Savoie Mont Blanc, CNRS, IRD, IFSTTAR, ISTerre, 38000 Grenoble, France*
[f] *Istituto Nazionale di Geofisica e Vulcanologia, Centro Nazionale Terremoti, Rome, Italy*
[g] *Istituto Nazionale di Geofisica e Vulcanologia, Centro Nazionale Terremoti, c/o DICCA University of Genoa, Genoa, Italy*

ARTICLE INFO

ABSTRACT

The anisotropy of seismic velocities in the mantle, when integrated with high-resolution tomographic models and geologic information, can be used to detect active mantle flows in complex plate boundary areas, providing new insights on the impact of mantle processes on the topography of mountain belts. Here we use a densely spaced array of temporary broadband seismic stations to analyze the seismic anisotropy pattern of the western Alpine region, at the boundary between the Alpine and Apenninic slabs. Our results are supportive of a poly-phase development of anisotropic mantle fabrics, possibly starting from the Jurassic to present. Geophysical data presented in this work, and geologic evidence taken from the literature, indicate that: (i) fossil fabrics formed during Tethyan rifting may be still preserved within the Alpine and Apenninic slabs; (ii) mantle deformation during Apenninic slab rollback is not compensated by a complete toroidal flow around the northern tip of the retreating slab; (iii) the previously observed continuous trend of anisotropy fast axes near-parallel to the western Alpine arc is confirmed. We observe that this arc-parallel trend of fast axes is located in correspondence to a low velocity anomaly in the European upper mantle, beneath regions of the Western and Ligurian Alps showing the highest uplift rates. We propose that the progressive rollback of the Apenninic slab, in the absence of a counterclockwise toroidal flow at its northern tip, induced a suction effect at the scale of the supraslab mantle. The resulting mantle flow pattern was characterized by an asthenospheric counterflow at the rear of the unbroken Western Alps slab and around its southern tip, and by an asthenospheric upwelling, mirrored by low *P* wave velocities, that would have favored the topographic uplift of the Alpine belt from the Mont Blanc to the Mediterranean sea.

1. Introduction

The anisotropy of seismic velocities in the mantle, mainly controlled by the lattice-preferred-orientation of olivine crystals (Savage, 1999; Mainprice et al., 2000), is widely used to constrain the asthenospheric flow pattern around lithospheric slabs (e.g., Long and Becker, 2010). However, seismic fast-axis directions may mark either active or fossil mantle flows (e.g., Savage and Sheehan, 2000; Piromallo et al., 2006; Audet, 2013; Eakin et al., 2016). Active mantle flows have an impact on present-day topography of continents and mountain belts (Cloetingh and Willett, 2013; Faccenna et al., 2014), and can be further investigated by numerical models of mantle dynamics (e.g., Becker et al., 2006; Faccenda and Capitanio, 2012).

In the Central Mediterranean, the slab structure is particularly complex, and a number of studies have already analyzed the seismic anisotropy pattern around the Alpine and Apenninic slabs separately (e.g., Barruol et al., 2004, 2011; Lucente et al., 2006; Salimbeni et al., 2008, 2013; Qorbani et al., 2015). A major counterclockwise asthenospheric flow has been proposed to the west of the Alpine slab from the Western Alps to the Tyrrhenian sea (Barruol et al., 2004, 2011),

whereas another counterclockwise toroidal flow has been proposed by several authors around the northern tip of the Apennines (Vignaroli et al., 2008; Faccenna and Becker, 2010; Salimbeni et al., 2013). However, the scarcity of seismic anisotropy data at the boundary between the Alpine and Apenninic slabs, and the uncertainties in the determination of the slab structure (e.g. Lippitsch et al., 2003; Piromallo and Morelli, 2003; Kissling et al., 2006; Giacomuzzi et al., 2011; Zhao et al., 2016, 2016), have so far precluded a full understanding of the asthenospheric flow pattern and the potential dynamic topography implications in this complex plate-boundary area.

In order to fill this gap, we present here new seismic anisotropy data from the western Alpine region, based on the recordings of a densely spaced array of temporary broadband seismic stations deployed from the European foreland to the Po Plain (CIFALPS experiment; Zhao et al., 2016). The new observations of birefringence of core-refracted shear waves (SKS phase) are integrated with data from previous work (Barruol et al., 2004, 2011; Salimbeni et al., 2008, 2013) and interpreted in the light of the upper mantle structure provided by the recent high-resolution *P* wave tomography model by Zhao et al. (2016). Results are discussed within the framework of available geologic constraints and recent geodynamic reconstructions of the Cenozoic Adria-Europe plate boundary area (e.g., Vignaroli et al., 2008; Malusà et al., 2015), providing new insights on the potential impact of mantle processes on the topographic growth of orogenic belts.

2. Tectonic and geodynamic setting

The Central Mediterranean area includes several slabs interacting with the asthenospheric mantle at the boundary between the European and African plates (Jolivet and Faccenna, 2000; Handy et al., 2010). The upper mantle structure beneath the Alpine region is particularly complex (Fig. 1a) due to the presence of a S- to E-dipping European slab beneath the Central and Western Alps, and of two slabs dipping in opposite directions (SW and NE) that belong to the Adriatic microplate beneath the Apennines and the Dinarides (Lucente et al., 1999; Piromallo and Morelli, 2003; Giacomuzzi et al., 2011; Zhao et al., 2016; Hua et al., 2017). The Alpine, Apenninic and Dinaric subduction zones accommodated the broadly N–S post-Jurassic convergence between Europe and Adria/Africa, leading to the progressive closure of the Alpine Tethys in between (Jolivet and Faccenna, 2000; Malusà et al., 2015). After the final exhumation of the thick subduction complex of the Western Alps in the late Eocene (Lardeaux et al., 2006; Dumont et al., 2012; Zhao et al., 2015), the Apenninic slab progressively translated northward beneath the Alpine orogenic wedge, and possibly started interacting with the Alpine slab by the end of the Oligocene (Malusà et al., 2015, 2016a). The rollback of the Apenninic slab during the Neogene (green arrow in Fig. 1b) led to the scissor-type opening of the Ligurian-Provençal basin and associated counterclockwise rotation of Corsica-Sardinia in the Apenninic backarc, followed by the opening of the Tyrrhenian basin since the Tortonian (Jolivet and Faccenna, 2000; Faccenna et al., 2001). The resulting crustal and upper-mantle structures at the boundary between the Alps and the Apennines are thus particularly complex (Zhao et al., 2015, 2016; Malusà et al., 2017; Solarino et al., 2018) and such a complexity is possibly mirrored by the pattern of vertical motions derived from GPS data (e.g., Serpelloni et al., 2013; Walpersdorf et al., 2015). Topographic uplift in the Western Alps is greatest in the westernmost part of the Alpine metamorphic wedge (Briançonnais units) and in the External Massifs farther west (e.g., Mont Blanc and Pelvoux, Fig. 1b), with rates generally > 1 mm/yr (Walpersdorf et al., 2015; Nocquet et al., 2016). Ongoing topographic uplift also characterizes the Ligurian Alps (Serpelloni et al., 2013), as also attested by the progressive northward tilting of strath terraces and sedimentary strata of the overlying Tertiary Piedmont Basin (TPB in Fig. 1b). Moreover, the timing of topographic uplift in these areas is apparently unrelated to the timing of subduction (Cretaceous to Paleogene) and backarc basin opening (latest Oligocene to Miocene): the

Western Alps show a strong increase in exhumation rate over the last 2 Myr (Fox et al., 2015), the Ligurian Alps were progressively tilted and uplifted since the Messinian, and the Northern Apennines where rapidly uplifted during the Pliocene (Malusà and Balestrieri, 2012).

3. Methods and dataset

The temporary network of the CIFALPS experiment (China-Italy-France Alps Seismic survey, Zhao et al., 2016) includes 46 broadband seismic stations deployed along a linear WSW–ENE transect from SE France to NW Italy, and 9 additional stations installed to the north and to the south of the main profile (Fig. 2 and Table S1). Stations utilized for our analysis operated from July 2012 to September 2013. Spacing between stations along the main profile ranges from ~5 km in the Western Alps mountain range to ~10 km in the European foreland and in the western Po Plain. The seismic anisotropy properties of the upper mantle beneath each single station were analyzed using the azimuth of the fast axis (φ) and the delay time (dt) as a proxy for the preferred orientation of olivine *a* axes and for the thickness of the anisotropic layer (Silver et al., 1999). Starting from the whole recordings of the CIFALPS experiment, we extracted the waveforms of 40 teleseismic events with M > 5.8 (Table S2), selected within an epicentral window between 80° and 120° to enhance the SKS pulse, and rejecting those pulses affected by preceding S phases.

The analysis of the SKS pulse was performed in two steps. As a first step, an automated SKS-splitting method based on energy minimization on the transverse waveform component (Silver and Chan, 1991) was applied on the entire array to the 9 earthquakes with the highest Signal-to-Noise ratio (SNR). We used the same time window and bandpass filter (5–50 s) for each stations-event pair, obtaining 90 new SKS splitting measurements (marked by a "A" in Table S3), mostly for stations in the western part of the profile, and 15 for stations in the eastern part of the profile or off-profile. Then, we manually analyzed 31 additional events using the SplitLab software (Wüstefeld et al., 2008) to fill the gap in back-azimuthal coverage and homogenize the dataset for all of the stations. The SplitLab software allows estimating the splitting parameters by using two different techniques, the cross-correlation and the minimization of the energy on the transverse component (see Wüstefeld et al., 2008 for details), under the assumption that SKS rays cross through a horizontal anisotropy (Silver and Chan, 1991). We considered only measurements showing consistent results using both techniques, according to the indications of Wüstefeld and Bokelmann (2007). In particular, we selected those measurements with SNR > 3 and delay time < 3 s, and sufficiently high quality to satisfy the visual inspection performed by operators during manual revision. Null measurements were only considered in case of no energy on the transverse component or when splitting was precluded (e.g., in the case of fast axes oriented perpendicular or parallel to the back-azimuth of analyzed earthquakes). Differently from the automatic method, the manual analysis was performed considering, for each station-event pair, the proper time window (seconds before and after the SKS arrivals) and filter (bandpass with corner frequency between 1 and 100 s) performing the highest SNR of the measurement. The complete set of utilized filters is summarized in Tables S3 and S4.

Manual analysis was further extended to 13 permanent stations, belonging to the Italian National Seismic Network and to the Regional Seismic Network of northwestern Italy, that are located near the eastern termination of the CIFALPS array leading to a total of 2380 results. After the application of the selection criteria described above, we obtained a final dataset of 506 new SKS splitting measurements (Table S3) and 169 new null measurements (Table S4) that will be considered for interpretation.

We analyzed the vertical and lateral variations in anisotropy properties beneath selected stations based on the analysis of the Fresnel zone, taking into account the seismic ray paths at various depths (50, 100, 150 and 200 km) for a SKS phase with dominant period of 10 s
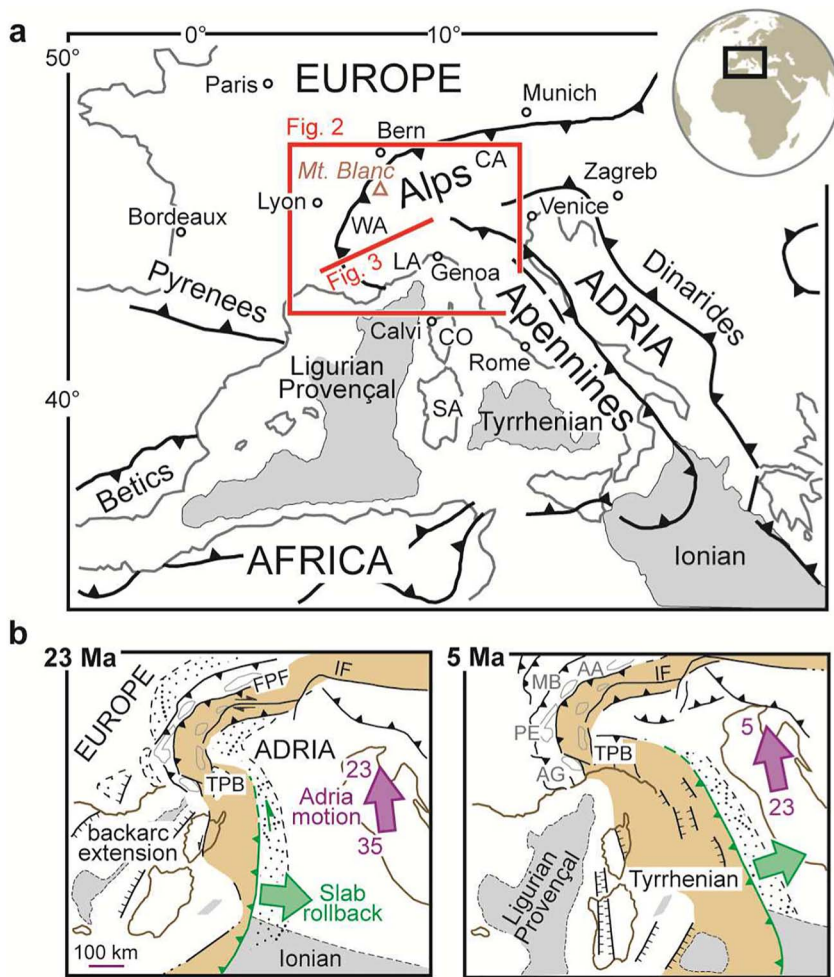
Fig. 1. a) Tectonic sketch map of the western Mediterranean, and location of the study area (in red; acronyms: CA, Central Alps; CO, Corsica; LA, Ligurian Alps; SA, Sardinia; WA, Western Alps). b) Neogene evolution of Alpine and Apenninic subductions (simplified after Malusà et al., 2015). Brown areas mark the metamorphic Alpine wedge and the Apenninic accretionary wedge; purple arrows indicate Adria trajectories relative to Europe (numbers = age in Ma); acronyms indicate the External Massifs (AA, Aar; AG, Argentera; MB, Mont Blanc; PE, Pelvoux), major faults (IF, Insubric Fault; FPF, Frontal Pennine Fault) and the Tertiary Piedmont Basin (TPB). (For interpretation of the references to color in this figure legend, the reader is referred to the web version of this article.)

(Alsina and Snieder, 1995; Margheriti et al., 2003). We used the formulation of Pearce and Mittleman (2002) and a shear wave velocity for S-phase as defined in the IASP91 model (4.48 km/s at 50 km depth, 4.49 km/s at 100 km depth, 4.45 km/s at 150 km depth and 4.51 km/s at 200 km of depth). By retrieving the ray paths of two teleseismic events arriving at the same station from opposite back-azimuths and sampling different fast-axis directions, we thus determined the minimum depth of lateral anisotropic variations.

4. Results

Results of our single SKS splitting measurements along the CIFALPS profile, and in the Po Plain farther east, are shown in Fig. 2. Measurements are projected at the 150 km piercing point depth, and are plotted as shades-of-blue segments parallel to the fast axis and scaled with the delay time, according to a color scale indicating the back-azimuth of the event, i.e. the incoming direction of the seismic ray at the station. Shear wave splitting data from previous works are plotted in yellow for comparison (Barruol et al., 2004, 2011; Salimbeni et al., 2008, 2013). Measurements lying within a 60-km-wide swath parallel to the CIFALPS profile (indicated in green in Fig. 2) are additionally plotted along the cross section of Fig. 3a.

Along the western part of the CIFALPS transect, teleseismic events yielded good quality results from all available back-azimuths. Fast-axes show NW–SE to WNW–ESE directions, and are part of a continuous trend of fast axes that follows the shape of the Alpine arc in the northern and western parts of the map of Fig. 2, from NE–SW in the Central Alps, to N–S in the northern Western Alps, and NW–SE in the southern Western Alps. This trend was first described by Barruol et al.

(2004, 2011), and finds its prolongation along the French Mediterranean coast and the Ligurian Alps, where fast-axes have WNW–ESE to E–W trends. Our new measurements in the Ligurian Alps, north of Genoa, show NE–SW and NW–SE fast-axis directions in agreement with previous data.

Along the eastern part of the CIFALPS transect, and more generally in the whole central part of the map of Fig. 2, measurements show variable fast-axis directions, and NE–SW, E–W and NW–SE directions are all equally frequently sampled (see rose diagrams in Fig. 3c). The percentage of good quality results is lower than in the western part of the map, due to the impact of the thick sedimentary cover of the Po Plain on the quality of the waveforms (see Fig. S2). In the southeastern part of the map, corresponding to the Northern Apennines (Fig. 2), the fast-axis directions define a broadly N–S trend north of Florence, and a NW–SE trend between Florence and Genoa, where our new data are consistent with those published by Salimbeni et al. (2008, 2013).

Variations in shear wave splitting parameters are clearer when data are projected onto a cross section parallel to the CIFALPS profile (Fig. 3). This allows to distinguish three different parts of the profile, labelled as western, central and eastern segments in Fig. 3a. The western segment of the profile (stations 1–17) shows quite homogeneous fast-axis directions in the range of $-60° \pm 20°$ (pale to dark blue marks in Fig. 3a), with minor differences depending on the back-azimuth of analyzed events (see Fig. 3c). The distribution of single fast-axis directions is also confirmed by the distribution of average fast-axis directions calculated for stations having at least 6 splitting measurements (red stars in Fig. 3a). Ray paths coming from the west (dark blue marks in Fig. 3a) show a trend of delay time that increases from 1 to 1.5 s in the westernmost 100 km to 2.4 s at ~140 km, and linearly
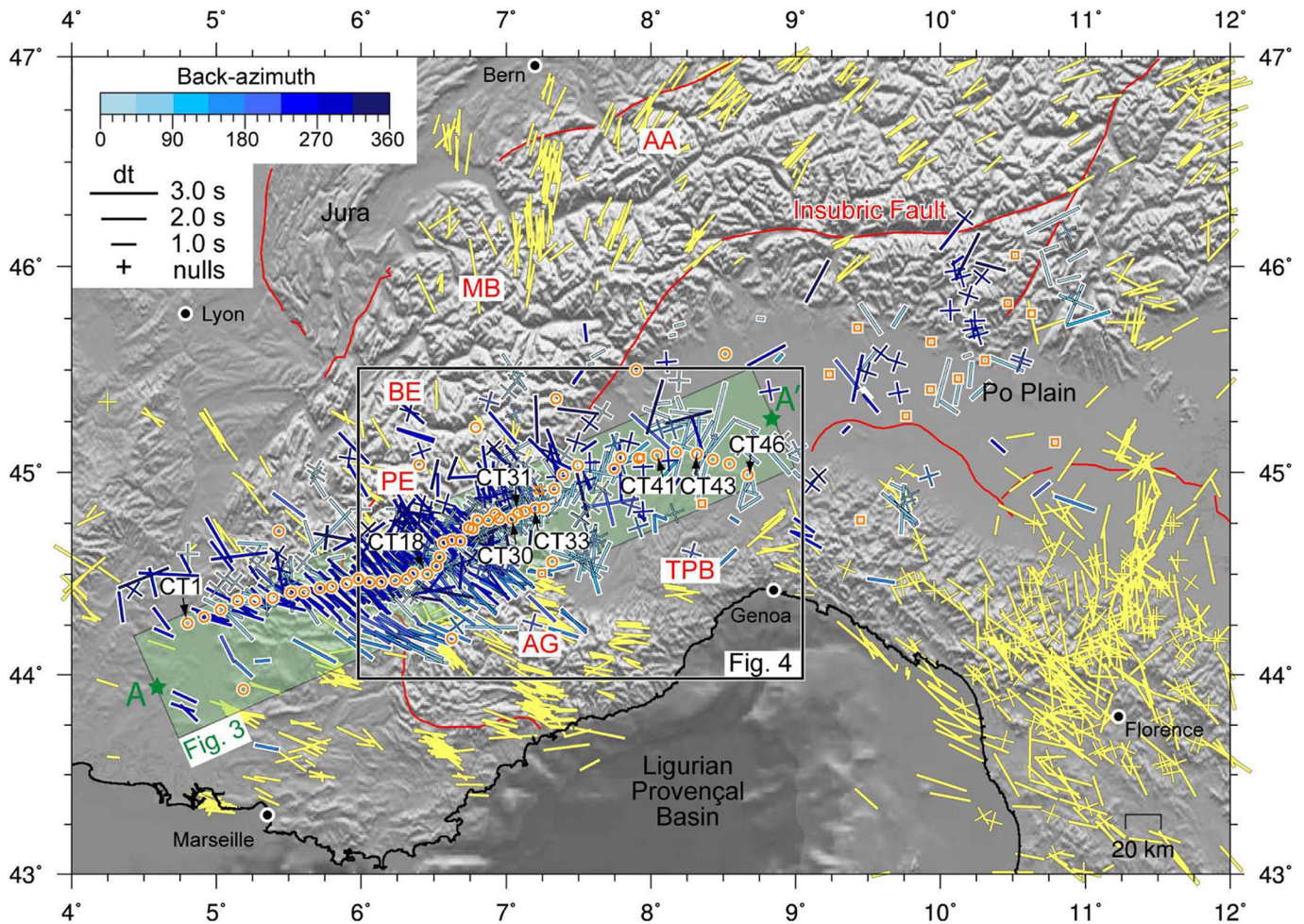
Fig. 2. Map of single SKS splitting measurements (blue = this work; yellow = previous works). Each measurement is plotted at 150 km depth as a segment parallel to the fast axis and scaled with delay time; null measurements are plotted as a cross with segments oriented parallel and perpendicular to the back-azimuth (see color scale for the back-azimuth of analyzed events). Seismic stations from the CIFALPS experiment (orange circles) and additional stations from permanent networks utilized in this work (orange squares) are also shown. Literature data are from Barruol et al. (2004, 2011) and Salimbeni et al. (2008, 2013) (datasets from Barruol et al., 2004, 2011 do not include null measurements). Acronyms: AA, Aar; AG, Argentera; BE, Belledonne; MB, Mont Blanc; PE, Pelvoux; TPB, Tertiary Piedmont Basin. (For interpretation of the references to color in this figure legend, the reader is referred to the web version of this article.)

decreases farther east.

In the central segment of the profile (stations 18–31), ray paths coming from the west sample a dominant NW–SE direction, whereas those coming from the east sample fast-axis directions with more dispersed trends, not only E–W to NW–SE, but also NNE–SSW (see Fig. 3c). Ray paths coming from the west (dark blue marks in Fig. 3a) define a trend of linearly decreasing delay times, from 2.4 s at 140 km, to 1.0 s at 220 km. This trend is not observed farther east.

In the eastern segment of the profile (stations 32–46), the fast-axis directions are even more dispersed (see also the average values marked by red stars in Fig. 3a), and show dominant N–S and NE–SW directions depending on the back-azimuth (Fig. 3c). Delay time is strongly scattered in the range from < 1 s to 2.8 s. Teleseismic events coming from the west mainly capture a N–S trend, whereas those coming from the east yield a maximum frequency of NNE–SSW fast-axis directions (see Fig. 3c). Null measurements (empty dots in Fig. 3a) are quite common in the central and eastern segments of the CIFALPS profile, as well as farther east in the Po Plain (see Table S4). A few null measurements are also found along the western segment of the CIFALPS profile, between abscissae 50 and 100 km (Fig. 3a).

The results of Fresnel zone analysis for stations CT30 and CT33 are shown in Fig. 4. In both stations, rays coming from NE have a 30° fast-axis direction, whereas rays coming from SW have a −50° fast-axis direction. At station CT30, the Fresnel zones around the ray piercing

points partly overlap at 50 km depth (orange circles in Fig. 4b), whereas they are fully separated at greater depths, pointing to an anisotropy source located at depth > 50 km. At station CT33, the Fresnel zones partly overlap at 50 and 100 km depth (orange and green circles in Fig. 4c), pointing to a source of anisotropy at depth > 100 km. The same considerations can be made for stations CT29, CT31, CT32 and CT35 (see Supplementary Fig. S1b) where we have enough information to calculate the Fresnel Zone, and where we obtained similar results. These results are in agreement with the Fresnel zone analysis performed by Barruol et al. (2011) from two stations (see their Fig. 6), and confirm that the change in seismic anisotropy pattern observed between the central and eastern segments of the CIFALPS profile is due to the sampling of different mantle regions and does not reflect a crustal contribution, as also suggested by the high values of delay time. Farther east in the Po Plain, Fresnel zone analysis from two stations (CT41 and CT43) is supportive of an additional lithospheric contribution to the observed anisotropy pattern, from depths shallower than 50 km (see Supplementary Fig. S1a). However, SKS measurements, for their characteristics and the strong heterogeneity of the measured anisotropy directions in the Po Plain, do not allow to locate this shallower contribution more precisely.
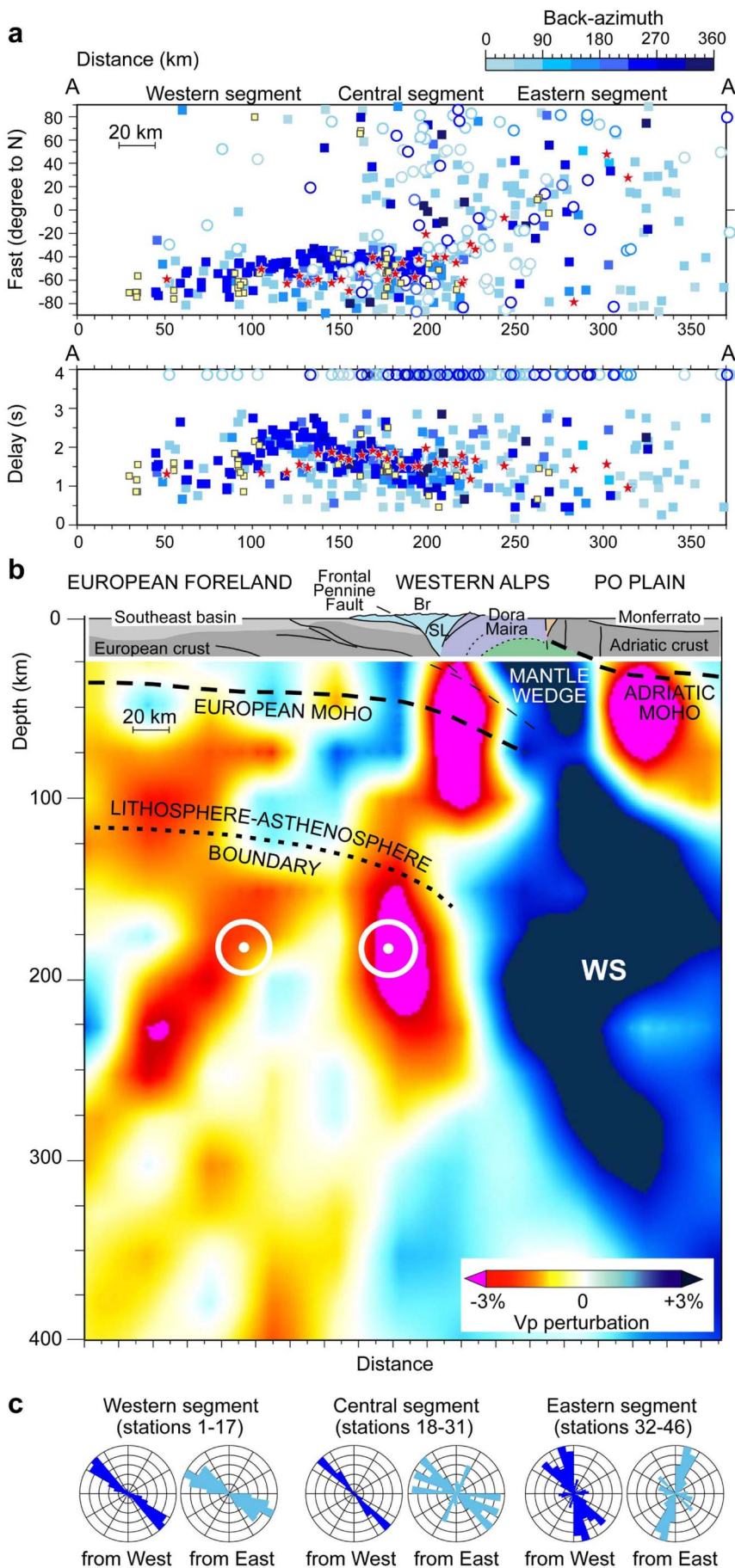
Fig. 3. a) Distribution of fast axes and delay times along a 60-km-wide swath following the CIFALPS transect (see location in Fig. 2). Full squares are splitting measurements from this work (in blue) and previous works (in yellow; from Barruol et al., 2004, 2011, Salimbeni et al., 2008, 2013); empty circles are null measurements, plotted as fast axes parallel to the back-azimuth and dt equal to 4 s. The color of markers depends on the event back-azimuth. Red stars indicate average fast-axis directions calculated for stations having at least 6 splitting measurements. Note the sharp change in fast axis orientation and delay time beneath the Western Alps, in the central segment of the CIFALPS profile. b) From top to bottom: (i) geologic cross-section along the CIFALPS transect (Br, Briançonnais; SL, Schistes lustrés); (ii) depth and geometry of the European and Adriatic Mohos based on receiver-function analysis (from Zhao et al., 2015), depth of the lithosphere-asthenosphere boundary based on array analysis of surface waves (from Lyu et al., 2017), and exhumed mantle wedge beneath the Dora-Maira based on local earthquake tomography (from Solarino et al., 2018); (iii) velocity structure of the underlying upper mantle based on finite-frequency P wave tomography (from Zhao et al., 2016). Low velocity anomalies (yellow to red) are located to the west of the Western Alps slab (WS), beneath the core of the Western Alps and the European foreland. White circles correspond to the asthenospheric counterflow illustrated in Fig. 5. c) Rose diagrams of fast-axis directions in the western, central and eastern segments of the CIFALPS profile (west and east back-azimuths). (For interpretation of the references to color in this figure legend, the reader is referred to the web version of this article.)
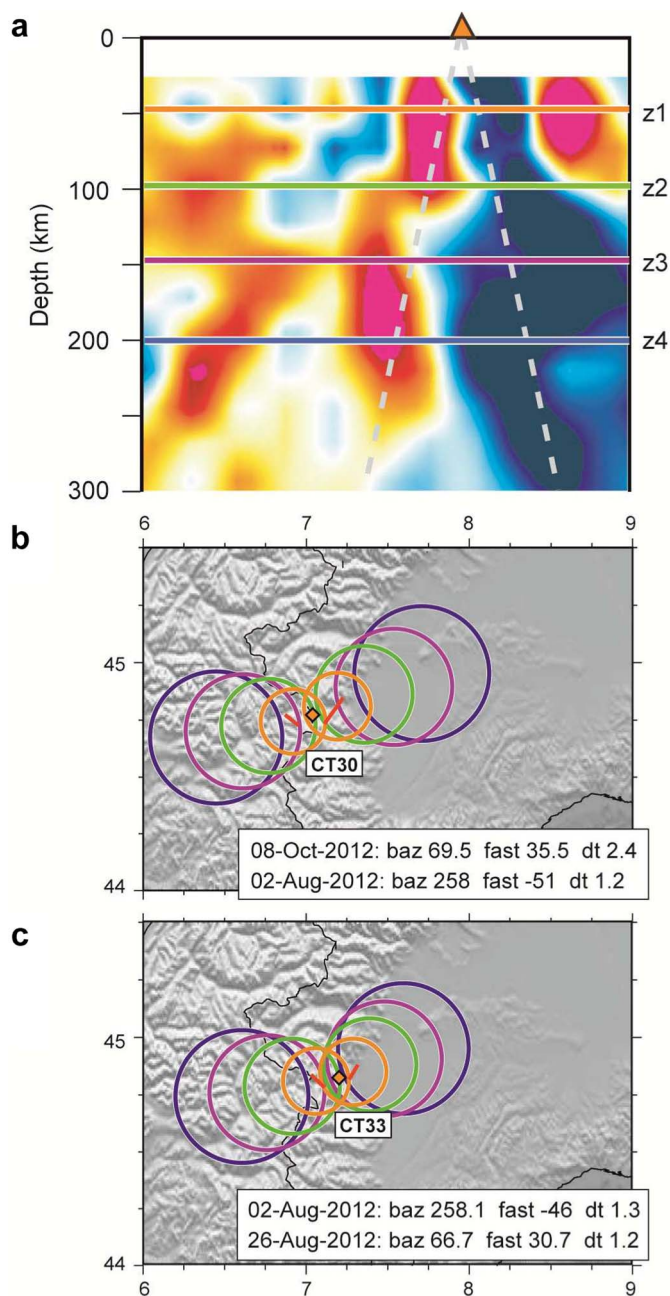
Fig. 4. Results of Fresnel zone analysis for ray paths emerging at the boundary between the Western Alps slab and the European asthenospheric mantle. a) Idealized ray paths for stations CT30 and CT33 (orange triangle) plotted on the tomographic cross section of Zhao et al. (2016). Lines in color show the depths (z1 to z4) analyzed in map view. b–c) Map views showing the Fresnel zones of analyzed ray paths at depths of 50 km (orange), 100 km (green), 150 km (purple) and 200 km (blue). Circles are scaled with the diameter of the Fresnel zone. The anisotropic parameters for each station-event pair (in red, details in map inset) are projected at 50 km depth. (For interpretation of the references to color in this figure legend, the reader is referred to the web version of this article.)

5. Comparison with *P* wave tomography data

Seismic anisotropy data are plotted in Fig. 5a onto the high-resolution *P* wave tomography model of Zhao et al. (2016). Colors in the 150 km depth slice of the tomography model indicate low-velocity (red to yellow) and high-velocity (light to dark blue) anomalies, the latter corresponding to the traces of the Central and Western Alps slabs (CS and WS) and Apenninic (Adriatic) slab (AS) at 150 km depth. The location of the high-velocity anomalies in the tomography model of Zhao et al. (2016) shows no major variation in the whole depth range

relevant for our seismic anisotropy study. In fact, both the Alpine and the Adriatic slabs dip almost vertically in the upper mantle of the study region. Any depth slice would thus show the same relationships between velocity anomalies and anisotropy as those shown in Fig. 5a.

Two main low-velocity anomalies are imaged in the map of Fig. 5a, the first one located to the west of the Alpine slab, running from western Switzerland to SE France and the Ligurian coast, and the second one located in the eastern part of the map, to the north of the Apenninic slab. The low-velocity anomaly located to the west of the Alpine slab is particularly evident at 100–250 km depth (see cross section in Fig. 3b) and can be recognized, with lower amplitudes, down to the mantle transition zone (Zhao et al., 2016). A comparison between *P* wave tomography and anisotropy data was already performed by Barruol et al. (2011) using the tomography model of Piromallo and Morelli (2003) and a dataset of 644 anisotropy measurements for the European mantle. When compared to the tomography model of Zhao et al. (2016), the tomography model of Piromallo and Morelli (2003) shows major differences that may influence the interpretation of the anisotropy pattern of the study area. In the Piromallo and Morelli (2003)'s model: (i) the low-velocity anomaly imaged to the west of the Alpine slab is discontinuous, unlike shown in our Fig. 5; (ii) the high-velocity anomaly corresponding to the Alpine slab would have a southwestern tip along the French Mediterranean coast, which implies that the slab would be crosscut by the continuous trend of fast axes running to the west of the Alpine arc (cf. Barruol et al. (2011), their Fig. 4b); (iii) the Alpine and Apenninic slabs would be separated by a major low-velocity gap, which is not observed in Zhao et al., 2016 (see Fig. 5a). All of these features, as well as other features such as the broken Alpine slab proposed by Lippitsch et al. (2003), were dismissed by the higher-resolution tomography model used in this work, and the interpretation of the mantle flow pattern was consequently improved.

When our seismic anisotropy dataset is compared with the tomography model of Zhao et al. (2016), the majority of null measurements observed in the Po Plain are clustered within the high-velocity anomalies corresponding to the Alpine and Apenninic slabs (blue areas in Fig. 5a). These regions of high-velocity anomaly also show slab-parallel and oblique fast-axis directions, the former mainly in correspondence to the Western Alps and Apenninic slabs, and the latter mainly in correspondence to the Central Alps slab. The complexity of the anisotropy pattern in these blue regions may result from the complexity of the medium traversed by the SKS waves: for example, waves recorded in the Po Plain stations may have crossed the Alpine slab as well as the overlying and underlying mantle (Figs. 3 and 4). A large number of nulls may thus result from such a complex path. Moreover, seismic anisotropy in the blue regions of Fig. 5a may also reflect fossil fabrics in the lithospheric mantle of the Alpine and Apenninic slabs, possibly acquired during mantle exhumation prior to the opening of the Tethyan ocean in the Jurassic (Lemoine et al., 1986; Vissers et al., 1995; Piccardo and Vissers, 2007). This hypothesis is discussed in detail in Section 6.1.

The fast-axis directions observed north of Florence mainly range from NNW–SSE to NE–SW (see rose diagram Fig. 5b). According to the tomography model of Zhao et al. (2016), they lay within the low-velocity anomaly located north of the Apenninic slab. Fig. 5a also shows that the continuous trend of fast axes following the Alpine arc from the Central Alps to the Ligurian coast (large red arrow in the map) lays in correspondence with a continuous low-velocity anomaly unravelled by *P* wave tomography to the west of the Alpine slab. This trend of fast-axis directions does not cut the Alpine slab.

Finally, the abrupt change in seismic anisotropy pattern observed between the central and eastern segments of the CIFALPS profile occurs in close correspondence with the transition between the Alpine slab and the western low velocity anomaly. Null measurements are common in both segments of the profile, but may have different origin as they reflect different situations at depth. The lateral changes in anisotropy parameters, unravelled by Fresnel zone analysis beneath stations CT30
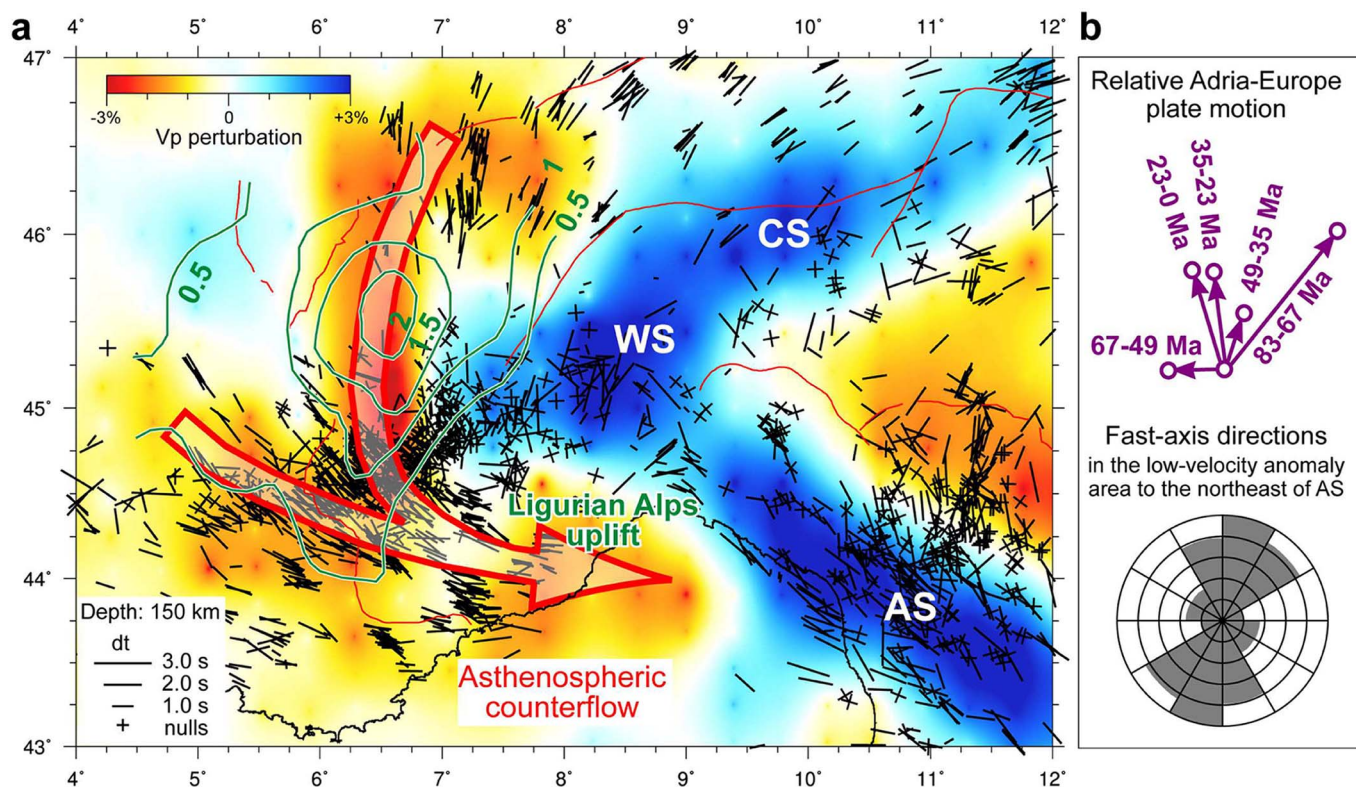
Fig. 5. a) Single shear wave splitting measurements (in black, projected to 150 km depth), and location of topographic uplift in the Western Alps (green contour lines = rates in mm/yr, after Nocquet et al., 2016) and in the Ligurian Alps, plotted onto the 150 km depth slice of the *P*-wave tomographic model of Zhao et al. (2016). Null measurements in the Po Plain are clustered within the slabs (blue background colors), which also show dominantly slab-parallel fast axes (AS, Apenninic slab; CS, Central Alps slab; WS, Western Alps slab). Major faults (red lines) as in Fig. 2. Note the correspondence between (i) the low velocity anomaly in the European upper mantle (yellow to red background colors in the western region of the map), (ii) the asthenospheric counterflow inferred from the orientation of fast axes (large red arrow), and (iii) the area of faster topographic uplift in the core of the Alps (green contour lines), which merges with the area of anomalous uplift in the Ligurian Alps (see text). b) Rose diagram of fast-axis directions, based on shear-wave splitting measurements in the area corresponding to the low-velocity anomaly north of the Apennines, attesting no toroidal flow around the northern tip of the Apenninic slab. Relative Adria-Europe plate motion after Dewey et al. (1989) (arrows are scaled with distance, numbers indicate the age in Ma). (For interpretation of the references to color in this figure legend, the reader is referred to the web version of this article.)

and CT33 at depth > 50–100 km (as well as beneath stations CT29, CT31, CT32 and CT35, see Supplementary Fig. S1b), are consistent with the presence of a steeply dipping slab beneath the eastern part of the CIFALPS profile (Fig. 4a). In the western and central segments of the CIFALPS profile, delay time variations for ray paths coming from the west (Fig. 3a) fit the pattern of *P* wave velocity perturbations (Fig. 3b). Lower delay times are found at abscissae 0–100 km and 150–200 km where the low-velocity anomaly in the mantle is stronger, whereas delay times are stronger at ~140 km where the low-velocity anomaly in the mantle is weaker (Fig. 3).

6. Discussion

6.1. Potential preservation of fossil fabrics within the Alpine and Apenninic slabs

Common patterns of trench-parallel fast directions along active margins, evidenced by shear-wave splitting measurements, are generally interpreted as the evidence of alignment of olivine crystals induced by mantle flow around downgoing slabs, whereas fossil fabrics within the slab are generally considered as a negligible source of anisotropy (Long and Silver, 2008, 2009; Audet, 2013). However, a fossil fabric defined by olivine crystallographic preferred orientation (CPO) can be preserved in the oceanic lithosphere since the time of plate formation (Mercier et al., 2008). This fossil fabric is generally aligned with the direction of plate spreading (Shinohara et al., 2008), and may either survive subduction-induced deformation (Audet, 2013), or be overprinted if the slab is sufficiently weak to undergo internal

deformation. Along-strike extension during flattening of the slab may lead to trench-parallel olivine CPO (Eakin et al., 2016), whereas the bending of the slab entering the trench may form vertically-aligned serpentinized faults in the uppermost slab portion (Faccenda et al., 2008). This would lead to trench-parallel fast directions resulting from both serpentine strong CPO (Bezacier et al., 2010) and larger-scale shape preferred orientation (SPO) determined by the alternation of dry and hydrated sections of mantle rocks (Faccenda et al., 2008).

When seismic anisotropy data of the western Alpine region are plotted onto the high-resolution *P* wave tomography model of Zhao et al. (2016) (Fig. 5a), the regions of high-velocity anomaly that are interpreted as slabs include a number of slab-parallel and oblique fast-axis directions. Here, we use available geologic and geodynamic constraints to explore the possibility that these fast-axis directions may reflect fossil fabrics in the lithospheric mantle of the Alpine and Apenninic slabs.

Fossil fabrics acquired during Tethyan rifting have long been recognized in mantle slivers accreted in orogenic belts of the Cenozoic Adria-Europe plate boundary (e.g., Nicolas et al., 1972; Vissers et al., 1995) (Fig. 6a). These mantle slivers mainly consist of coarse-grained spinel lherzolite tectonites displaying well-developed olivine CPO, consistent with deformation by dislocation creep (Tommasi et al., 1999; Vauchez et al., 2012). This tectonite fabric, developed at 900°–1000 °C and ~1.4 GPa (corresponding to depths of 40–45 km), is the result of low-angle simple shearing during Jurassic asymmetric rifting (Hoogerduijn Strating et al., 1993), and is expected to characterize a thick section of the slab. The tectonite fabric of exhumed spinel lherzolites is generally overprinted by spinel-, plagioclase-, hornblende- and
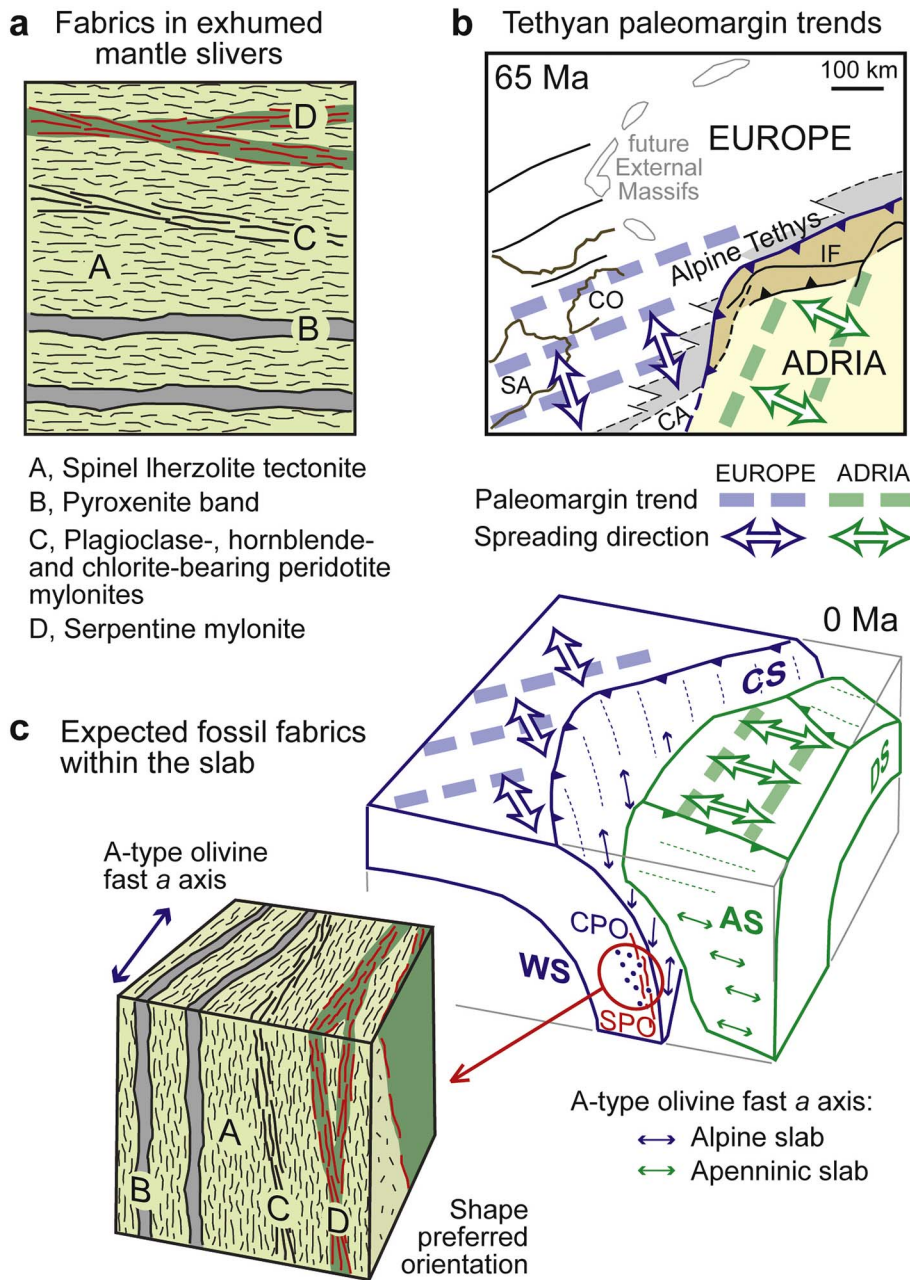
Fig. 6. a) Anisotropic fabrics inherited from the Tethyan rifting as observed in outcrops of exhumed mantle rocks within the Alpine orogenic wedge (Erro-Tobbio unit, e.g., Piccardo and Vissers, 2007 and references therein). b) Palinspastic reconstruction of the Cenozoic Adria-Europe plate boundary at 65 Ma (based on Malusà et al., 2015, 2016b) showing the trends of the European and Adriatic paleomargins and the inferred directions of Tethyan spreading (CA, Calabria; CO, Corsica; IF, Insubric Fault; SA, Sardinia). c) Expected attitude of fossil anisotropic fabrics within the Alpine and Apenninic slabs, based on the direction of plate spreading, trench orientation and slab dip (AS, Apenninic slab; CS, Central Alps slab; DS, Dinaric slab; WS, Western Alps slab). CPO = crystallographic preferred orientation; SPO = shape preferred orientation.

chlorite-bearing mylonites, developed as a result of strain localization during progressive mantle exhumation towards the Tethys seafloor (Piccardo and Vissers, 2007). Serpentine gently dipping mylonites overprint these rocks during the latest stages of mantle exhumation, at temperature < 500 °C, and are only expected in the uppermost portions of the slab (e.g. Guillot et al., 2015 for a review). Pervasive serpentinized faults, crosscutting perpendicularly these tectonite and mylonitic fabrics, and pre-dating subduction as postulated by Faccenda et al. (2008), are not documented in the geologic record of the Alps and the Apennines.

Because fabrics developed during Tethyan rifting are still preserved in rock slivers that underwent major deformation at eclogitic depths within the Alpine subduction channel (e.g., the Erro-Tobbio unit; Scambelluri et al., 1995; Hermann et al., 2000), we can infer that these fabrics are likely preserved within low-strain domains of the Alpine and Apenninic slabs, too. The attitude of these fabrics within the slab is of primary importance for the interpretation of shear-wave splitting measurements in the western Alpine region, and depends on: (i) the

direction of plate spreading in the Jurassic, (ii) the trench orientation relative to the paleomargin, and (iii) the present-day slab dip.

The direction of plate spreading in the Jurassic was likely perpendicular to the trend of the European and Adriatic paleomargins of the Tethys, which are independently constrained by a wealth of tectonic, stratigraphic and thermochronologic data (e.g., Winterer and Bosellini, 1981; Lemoine et al., 1986; Guillot et al., 2009; Fantoni and Franciosi, 2010; Malusà et al., 2016b). Available data consistently point to a NNW–SSE plate-spreading trend, with a progressive counterclockwise rotation from NNW–SSE to NW–SE in the Adriatic microplate accomplished during post-Jurassic Adria-Europe convergence (Fig. 6b). The orientations of the Alpine and Apenninic trenches are well constrained by *P* wave tomography models (Piromallo and Morelli, 2003; Zhao et al., 2016) and paleotectonic reconstructions. In the Western Alps segment of the Alpine trench, subduction was strongly oblique relative to the European paleomargin (Malusà et al., 2015), and the direction of plate spreading is consequently at low-angle to the trend of the trench (Fig. 6c). In the Central Alps segment of the Alpine trench, subduction

was near-parallel to the trend of the European paleomargin, and the direction of plate spreading is consequently near-perpendicular to the trench (Fig. 6c). Subduction in the Appennines was initially near-parallel to the Adriatic paleomargin (see Fig. 1b). However, during Neogene rollback of the Apenninic slab, the Apenninic trench progressively rotated towards its present-day NW–SE trend (Jolivet and Faccenna, 2000), which is parallel to the direction of plate spreading inferred for the Adriatic microplate (Fig. 6c). According to *P* wave tomography models (Zhao et al., 2016), both the Alpine and Apenninic slabs are now plunging near-vertically in the upper mantle.

Fig. 6c illustrates the expected attitude, within the steeply-dipping Alpine and Apenninic slabs, for the olivine CPOs of spinel lherzolite tectonites and for the larger-scale SPOs determined by the alternation between dry mantle rocks and serpentine mylonites formed during Tethyan rifting. Both in the Western Alps and Apenninic slabs, the fast *a* axes of A-type olivine should be near-parallel to the trench (Fig. 6c), in agreement with the trench-parallel fast directions derived from shear-wave splitting measurements (Fig. 5a). In the uppermost part of the slab, a similar polarization of seismic waves would be favored by the near-vertical attitude of tilted serpentine mylonites initially formed during Tethyan extension. Within the Central Alps slab, serpentine mylonites are still inferred to be near-vertical, but the different attitude of the olivine *a* axes may explain the more oblique fast-axis directions, relative to the slab, derived from shear-wave splitting measurements in the Central Alps area. Notably, part of the measurements reported in Fig. 5a may reflect not only the complex fossil fabric of the slab, but also the mantle structure below and above the slab (Figs. 3, 4). The resulting complex anisotropy signature may thus explain part of the null measurements of Fig. 5a.

In summary, based on available geologic and geodynamic constraints, preserved fossil fabrics within the Alpine and Apenninic slabs may satisfactorily explain the seismic anisotropy patterns documented within the areas of high-velocity anomaly in Fig. 5a. At the eastern termination of the CIFALPS transect, in the light of the relationships among fossil fabrics summarized in Fig. 6c, the transition from dominant NE–SW fast axes (to the west) to dominant NW–SE axis (to the east) may mark the boundary between the Alpine and Apenninic slabs (Fig. 5a).

6.2. No toroidal mantle flow north of the Apenninic slab

Several previous papers dealing with the geodynamics of the Central Mediterranean have postulated a counterclockwise toroidal mantle flow around the northern tip of Apenninic slab (e.g., Vignaroli et al., 2008; Faccenna and Becker, 2010). Such a toroidal flow would compensate the effects of Apenninic slab retreat on the adjoining asthenospheric mantle, by transferring mantle material from the rear of the retreating Apenninic slab towards a supraslab position in front of the SE-dipping Alpine slab (Vignaroli et al., 2008; Salimbeni et al., 2013). However, the seismic anisotropy data provided in this work are not supportive of an efficient toroidal flow in the study region. This is particularly clear when considering the area of low-velocity anomaly located north of the Apenninic slab (Fig. 5a). This area, under the hypothesis of a toroidal flow, should be characterized by dominant slab-parallel NW–SE fast-axis directions, progressively rotating around the northern tip of the Apenninic slab to yield dominant E–W to ENE–WSW fast-axis directions. As shown in the rose diagram of Fig. 5b, these directions are instead the least represented in the area to the north of the Apenninic slab, ruling out the hypothesis of a counterclockwise toroidal mantle flow around its northern tip. The only few measurements with a direction perpendicular to the Apenninic slab are located north of Genoa, exactly at the boundary between the two slabs, where the high-velocity anomaly in the tomography model of Zhao et al. (2016) is slightly weaker (Fig. 5a).

The typical distribution of seismic anisotropy directions in the case of toroidal flow in the asthenospheric mantle has been successfully described in various segments of the Apenninic slab that show evidence of a major slab window or a slab tear (Civello and Margheriti, 2004; Baccheschi et al., 2011). The tomography model of Fig. 5a, unlike previous models (e.g., Piromallo and Morelli, 2003), shows no evidence of a major gap in the slab structure between the Alps and the Apennines at upper mantle depths, in line with independent geologic evidence (Malusà et al., 2016a). The absence of space between the two slabs, as a result of Africa-Eurasia collision that put the system under compression and the two slabs in contact, may have precluded any flows around the northern tip of the Apenninic slab, with major implications, discussed in detail in Section 6.3, also for the asthenospheric flow pattern imaged to the west of the Alpine slab (Barruol et al., 2004, 2011).

Notably, the dominant NNW–SSE to NE–SW fast-axis directions in the region of low-velocity anomaly to the north of the Apenninic slab (Fig. 5a) are largely consistent with the direction of relative Adria-Europe plate motion inferred from magnetic anomalies since the Late Cretaceous (Fig. 5b) (Dewey et al., 1989; Jolivet and Faccenna, 2000). This suggests that the anisotropic fabric unravelled by shear-wave splitting measurements may have formed during post-Jurassic Adria-Europe convergence, and possibly before the onset of Apenninic slab rollback. The observation that WNW–ESE fast axes are poorly represented in the Po Plain beneath the Adriatic microplate is in agreement with the asymmetric configuration of the Tethyan rifting long-recognized from geologic evidence (Lemoine et al., 1986; Manatschal, 2004; Manatschal and Müntener, 2009; Malusà et al., 2015). Asymmetric rifting implies that tectonite fabrics, during lithospheric extension, are best developed within the Tethyan oceanic lithosphere and within the European subcontinental mantle, but are not expected to be widespread within the Adriatic subcontinental mantle, in line with the results of our SKS splitting measurements.

6.3. Insights on the asthenospheric flow around the Western Alps slab

Our seismic anisotropy analysis confirms the occurrence of a continuous trend of fast axes that follows, to the west of the Alpine slab, the whole arc of the Western Alps down to the Ligurian coast, where this trend merges with a WNW–ESE trend in part already described by Barruol et al. (2004) along the Mediterranean coast of SE France. Such seismic anisotropy pattern shows different directions compared to the azimuthal anisotropy from noise and surface waves in the same region, which sample a maximum depth of 120–125 km (Fry et al., 2010; Zhu and Tromp, 2013), and from the *Pn* anisotropy that samples the shallow lithospheric mantle (Díaz et al., 2013). Along the CIFALPS profile, the azimuthal anisotropy from surface waves invariably shows an E–W trend (see Zhu and Tromp, 2013, their Fig. 2), whereas the fast polarization directions of *Pn* anisotropy show a N–S trend along the western and central segments of the profile, and an E–W trend along the eastern segment of the profile (see Díaz et al., 2013, their Fig. 9). Therefore, the seismic anisotropy pattern that we obtain to the west of the Alpine slab can be safely ascribed to a re-orientation of the olivine fast axis within the European asthenospheric mantle.

Since its first detection, the seismic anisotropy pattern described along the Mediterranean coast of SE France was readily interpreted as an effect of asthenospheric flow due to the eastward retreat of the Apenninic slab (Barruol et al., 2004; Lucente et al., 2006; Jolivet et al., 2009), whereas the belt-parallel trend of fast axes around the Alpine arc was tentatively ascribed, in the absence of high-resolution tomographic images of the Alpine area, to a range of different geodynamic processes (Barruol et al., 2011), i.e.: (i) a possible toroidal flow induced by the keel effect of the Alpine slab during the motion of the European plate; (ii) a mantle flow around the sinking Alpine slab after slab detachment; or (iii) an effect of Alpine and Apenninic slab rollback. The hypothesis of a mantle flow around the detached Alpine slab is ruled out by the slab continuity attested by *P* wave tomography (Zhao et al., 2016), whereas the hypothesis of Alpine slab rollback is ruled out by independent geologic and paleomagnetic evidences (Handy et al., 2010;
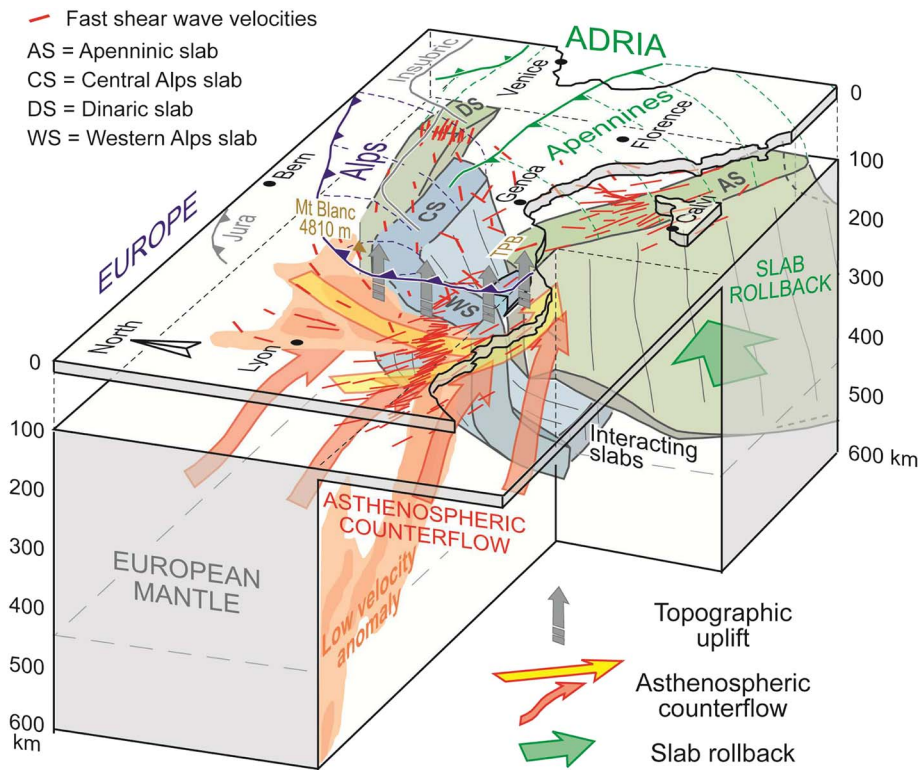
Fig. 7. Interpretive 3D model showing the relationships between slab structure, active mantle flow and topographic uplift in the Western and Ligurian Alps regions. The progressive rollback of the Apenninic slab, in the absence of a toroidal flow around its northern tip, induces a suction effect and asthenospheric counterflow at the rear of the unbroken Western Alps slab and around its southern tip. The temperature increase due to asthenospheric upwelling, mirrored by a low velocity anomaly in the European mantle (detected by *P* wave tomography), may have favored the topographic uplift from the Mt. Blanc to the Ligurian coast. Station-averaged shear wave splitting measurements are in red; slab structure and low velocity anomalies are after Zhao et al. (2016); TPB = Tertiary Piedmont basin.

Malusà et al., 2015).

The observed correspondence between the continuous trend of fast axes parallel to the trend of the Alpine arc (large red arrow in Fig. 5a) and the low velocity anomaly in the European upper mantle (yellow to red background colors in Fig. 5a) allows a refined interpretation of the mantle flow pattern to the west and beneath the Western Alps. The westward-plunging low-velocity anomaly may be generated by the presence of fluids, or may have a thermal origin. The former hypothesis can be excluded in the light of the location and the depth of the anomaly with respect to the nearby slabs. A potential thermal origin may be due to asthenospheric upwelling, possibly related to a counterflow induced by the retreat of the Apenninic slab in the absence of an adequate mass compensation by a toroidal mantle flow (Fig. 7). The mantle upwelling hypothesis is consistent with the delay-time pattern observed in the western and central segments of the CIFALPS profile. In fact, the shorter time delays are found where the low-velocity anomaly is stronger (Fig. 3), which may indicate that the anisotropy is not fully confined within the horizontal plane (e.g., Savage and Sheehan, 2000). The same relationships between delay times and velocity structure based on finite-frequency *P* wave tomography is also observed in map view in Fig. 5a. Moving from the western to the central segment of the CIFALPS profile, the number of null measurements increases drastically, and the fast-axis directions start to become more scattered, all clues pointing to the presence of a possible vertical component of the mantle flow in that area (Long and Becker, 2010; Díaz et al., 2013). A better characterization of the inferred vertical component of the mantle flow around the Western Alps slab would require a combined analysis of Love and Rayleigh waves that is beyond the aims of this work. Its magnitude is probably much smaller than the magnitude of the long-recognized horizontal component, but anyway of great consequence. We speculate that such vertical mantle-flow component, progressively propagating towards the east during the Neogene rollback of the Apenninic slab (Fig. 1b), determined a temperature increase in the vicinity of the retreating slab that may be responsible for the low-velocity anomaly imaged by *P* wave tomography (Zhao et al., 2016).

6.4. Hypothesis of a linkage between asthenospheric counterflow and topographic uplift

The Western Alps include the highest summits in Europe, but factors controlling their topographic uplift still remain poorly understood. Convergence rates in the western Alpine area are below the detection limit (Calais et al., 2002), ruling out a primary control of horizontal plate motion on topography development. GPS and levelling measurements (e.g. Walpersdorf et al., 2015) unravel a pattern of rock uplift with rates locally > 2 mm/yr that are only partly explained by the isostatic response to erosion and glaciation (Chéry et al., 2016; Nocquet et al., 2016; Nguyen et al., 2016). Thermochronologic data (e.g. Fox et al., 2015) show that the areas with highest uplift rates have also experienced the highest long-term erosion rates during the Neogene, ruling out the hypothesis of a crustal-scale collapse of the mountain range previously suggested on the basis of structural analysis and earthquake focal mechanisms (Champagnac et al., 2004; Selverstone, 2005). In the absence of active convergence, recent works suggested that the highest rates of rock uplift and erosion in the Western Alps might be a surficial response to European slab breakoff (Sue et al., 1999; Fox et al., 2015; Nocquet et al., 2016). However, this latter hypothesis is ruled out by the down-dip continuity of the European slab documented by recent high-resolution tomographic images of the upper mantle beneath the Alpine region (Zhao et al., 2016). Toroidal flow has been also suggested as a potential player controlling topography development and mantle upwelling next to retreating slab edges (e.g., Piromallo et al., 2006; Zandt and Humphreys, 2008; Schellart, 2004, 2010; Faccenna and Becker, 2010; Long et al., 2012). Data presented in this work are not supportive of a complete toroidal mantle flow around the northern edge of the retreating Apenninic slab. However, our data may suggest an alternative mantle driver for Alpine topography. The map of Fig. 5a shows a good correspondence not only between the asthenospheric counterflow inferred from seismic anisotropy analysis and the low velocity anomaly imaged by *P* wave tomography, but also with the area of faster topographic uplift in the core of the Western Alps (green contour lines in Fig. 5a) and with the area of anomalous uplift in

the Ligurian Alps, which are flanked to the south by a Neogene backarc basin. The observed uplift rates beneath the External Massifs and the Briançonnais units cannot be simply explained by tectonic shortening or by an isostatic response to erosion and deglaciation (Calais et al., 2002; Chéry et al., 2016; Nocquet et al., 2016). Moreover, the Ligurian Alps were neither affected by glaciations, nor by major tectonic shortening (Malusà et al., 2015). Our results suggest that Apenninic slab rollback, in the absence of a toroidal flow around the northern tip of the Apenninic slab, may have induced not only a suction effect and an asthenospheric counterflow at the rear of the unbroken Western Alps slab and around its southern tip, but also an asthenospheric upwelling in the same region, leading to a temperature increase in the upper mantle. As already discussed by Nocquet et al. (2016), the replacement of a dense and cold mantle material by hot and buoyant asthenospheric mantle at the base of the European lithosphere (estimated at 100 km depth, Lyu et al., 2017) would induce uplift. Furthermore, the weakening of the lithosphere and the lower crust by asthenospheric heat advection, as documented in the cross-section of Fig. 3b, can also foster Alpine uplift (Chéry et al., 2016). The occurrence of hot springs in the core of the Western and Ligurian Alps (Marty et al., 1992), right above the low-velocity anomaly, are also supportive of a focused thermal anomaly.

A deep control of Alpine topography, in the light of the inferred thermal origin for the low-velocity anomaly detected by P wave tomography, may explain the higher average elevation of the Western Alps compared to other segments of the Alpine belt located farther east (i.e., the central and eastern Alps). However, it is unlikely that the elevated topography of the External Massifs and the Briançonnais is exclusively due to a mantle driver, and a role may also be played by along-strike lithological changes and the presence of the Ivrea body (Liao et al., 2018). A first-order estimate of the relative impact of mantle vs surface processes in determining topographic uplift can be attempted by comparing the present-day uplift rates in the glaciated and rapidly eroded Western Alps areas with those of the Ligurian Alps, where tilting of the overlying Tertiary Piedmont strata is associated to minor erosion, and the impact of glaciations is minor. In the Ligurian Alps, cosmogenic data (Wittmann et al., 2016) point to uplift rates not greater than ~0.4 mm/yr that are likely ascribed to a mantle driver. A full understanding of the impact of mantle processes in shaping the Alpine topography, compared to surface processes and crustal-scale tectonic processes, would now require a numerical modelling of dynamic topography based on the recent high-resolution P wave tomography of the Alpine region and the pattern of active mantle flow highlighted in this work.

7. Conclusion

The seismic anisotropy pattern in the western Alpine region, when interpreted within the framework of the upper mantle structure unravelled by high-resolution P wave tomography complemented with available geologic and geodynamic constraints, unravels a polyphase development of anisotropic fabrics in the mantle of the western Alpine area. Fossil fabrics formed during Tethyan rifting are possibly preserved within the Alpine and Apenninic slabs, which would suggest that these slabs are sufficiently stiff and did not undergo major internal deformation during the Cenozoic. The Neogene rollback of the Apenninic slab was not compensated by a complete toroidal flow in the upper mantle around the northern tip of the retreating slab. This finding has major implications for the asthenospheric flow pattern imaged to the west of the Alpine slab. The continuous trend of seismic anisotropy fast axes, which follows the whole arc of the Western Alps down to the Ligurian coast, marks the horizontal component of an asthenospheric flow developed as a response to Apenninic slab rollback, and recognized from the fore-arc side of the Alpine slab to the backarc of the Apenninic slab. The low-velocity anomaly detected by P wave tomography in the upper mantle beneath the Western Alps can be ascribed to

a temperature increase due to the vertical component of such asthenospheric flow, which may have favored the topographic uplift of the overlying lithosphere. Our results suggest that the impact of mantle flow in response to active subduction may foster the topographic uplift of distant orogenic belts, where subduction processes have been inactive for several millions of years.

Appendix A. Supplementary data

Supplementary data to this article can be found online at https://doi.org/10.1016/j.tecto.2018.03.002.

References

Alsina, D., Snieder, R., 1995. Small-scale sublithospheric continental mantle deformation; constraints from SKS splitting observations. Geophys. J. Int. 123, 431–448.

Audet, P., 2013. Seismic anisotropy of subducting oceanic uppermost mantle from fossil spreading. Geophys. Res. Lett. 40 (1), 173–177.

Baccheschi, P., Margheriti, L., Steckler, M.S., Boschi, E., 2011. Anisotropy patterns in the subducting lithosphere and in the mantle wedge: a case study—the southern Italy subduction system. J. Geophys. Res. 116, B08306. http://dx.doi.org/10.1029/2010JB007961.

Barruol, G., Bonnin, M., Pedersen, H., Bokelmann, G., Tiberi, C., 2011. Belt-parallel mantle flow beneath a halted continental collision: the Western Alps. Earth Planet. Sci. Lett. 302, 429–438.

Barruol, G., Deschamps, A., Coutant, O., 2004. Mapping upper mantle anisotropy beneath SE France by SKS splitting indicates a Neogene asthenospheric flow induced by the Apenninic slab rollback and deflected by the deep Alpine roots. Tectonophysics 394, 125–138.

Becker, T.W., Chevrot, S., Schulte-Pelkum, V., Blackman, D.K., 2006. Statistical properties of seismic anisotropy predicted by upper mantle geodynamic models. J. Geophys. Res. Solid Earth 111 (B8).

Bezacier, L., Reynard, B., Bass, J.D., Sanchez-Valle, C., Van de Moortèle, B., 2010. Elasticity of antigorite, seismic detection of serpentines, and anisotropy in subduction zones. Earth Planet. Sci. Lett. 289 (1), 198–208.

Calais, E., Nocquet, J.M., Jouanne, F., Tardy, M., 2002. Current strain regime in the Western Alps from continuous global positioning system measurements, 1996–2001. Geology 30, 651–654.

Champagnac, J.D., Sue, C., Delacou, B., Burkhard, M., 2004. Brittle deformation in the inner NW Alps: from early orogen-parallel extrusion to late orogen-perpendicular collapse. Terra Nova 16, 232–242.

Chéry, J., Genti, M., Vernant, P., 2016. Ice cap melting and low-viscosity crustal root explain the narrow geodetic uplift of the Western Alps. Geophys. Res. Lett. 43. http://dx.doi.org/10.1002/2016GL067821.

Civello, S., Margheriti, L., 2004. Toroidal mantle flow around the Calabrian slab (Italy) from SKS splitting. Geophys. Res. Lett. 31, L10601. http://dx.doi.org/10.1029/2004GL019607.

Cloetingh, S., Willett, S.D., 2013. TOPO-EUROPE: understanding of the coupling between the deep Earth and continental topography. Tectonophysics 602, 1–14.

Dewey, J.F., Helman, M.L., Turco, E., Hutton, D.H.W., Knott, S.D., 1989. Kinematics of the western Mediterranean. In: Coward, M.P., Dietrich, D., Park, R.G. (Eds.), Alpine Tectonics. Geol. Soc. London Spec. Publ. 45pp. 265–283.

Díaz, J., Gil, A., Gallart, J., 2013. Uppermost mantle seismic velocity and anisotropy in the Euro-Mediterranean region from Pn and Sn tomography. Geophys. J. Int. 192, 310–325.

Dumont, T., Schwartz, S., Guillot, S., Simon-Labric, T., Tricart, P., Jourdan, S., 2012. Structural and sedimentary records of the Oligocene revolution in the Western Alps. J. Geodyn. 56–57, 18–38.

Eakin, C.M., Long, M.D., Scire, A., Beck, S.L., Wagner, L.S., Zandt, G., Tavera, H., 2016. Internal deformation of the subducted Nazca slab inferred from seismic anisotropy. Nat. Geosci. 9 (1), 56–59.

Faccenda, M., Burlini, L., Gerya, T.V., Mainprice, D., 2008. Fault-induced seismic

anisotropy by hydration in subducting oceanic plates. Nature 455, 1097–1100.

Faccenda, M., Capitanio, F.A., 2012. Development of mantle seismic anisotropy during subduction-induced 3-D flow. Geophys. Res. Lett. 39 (11), L11305.

Faccenna, C., Becker, T.W., 2010. Shaping mobile belts by small scale convection. Nature 465, 505–602. http://dx.doi.org/10.1038/nature09064.

Faccenna, C., Becker, T.W., Auer, L., Billi, A., Boschi, L., Brun, J.P., Capitanio, F.A., Funiciello, F., Horvàth, F., Jolivet, L., Piromallo, C., Royden, L., Rossetti, F., Serpelloni, E., 2014. Mantle dynamics in the Mediterranean. Rev. Geophys. 52, 283–332.

Faccenna, C., Becker, T.W., Lucente, F.P., Jolivet, L., Rossetti, F., 2001. History of subduction and back arc extension in the Central Mediterranean. Geophys. J. Int. 145, 809–820.

Fantoni, R., Franciosi, R., 2010. Tectono-sedimentary setting of the Po Plain and Adriatic foreland. Rend. Lincei 21 (1), 197–209.

Fox, M., Herman, F., Kissling, E., Willett, S.D., 2015. Rapid exhumation in the Western Alps driven by slab detachment and glacial erosion. Geology 43 (5), 379–382.

Fry, B., Deschamps, F., Kissling, E., Stehly, L., Giardini, D., 2010. Layered azimuthal anisotropy of Rayleigh wave phase velocities in the European Alpine lithosphere inferred from ambient noise. Earth Planet. Sci. Lett. 297, 95–102.

Giacomuzzi, G., Chiarabba, C., De Gori, P., 2011. Linking the Alps and Apennines subduction systems: new constraints revealed by high-resolution teleseismic tomography. Earth Planet. Sci. Lett. 301, 531–543.

Guillot, S., di Paola, S., Ménot, R.P., Ledru, P., Spalla, M.I., Gosso, G., Schwartz, S., 2009. Suture zones and importance of strike-slip faulting for Variscan geodynamic reconstructions of the external crystalline massifs of the western Alps. Bull. Soc. Geol. Fr. 180 (6), 483–500.

Guillot, S., Schwartz, S., Agard, P., Renard, B., Prigent, C., 2015. Tectonic significance of serpentinites. Tectonophysics 646, 1–19.

Handy, M.R., Schmid, S.M., Bousquet, R., Kissling, E., Bernoulli, D., 2010. Reconciling plate-tectonic reconstructions of Alpine Tethys with the geological–geophysical record of spreading and subduction in the Alps. Earth Sci. Rev. 102, 121–158.

Hermann, J., Müntener, O., Scambelluri, M., 2000. The importance of serpentinite mylonites for subduction and exhumation of oceanic crust. Tectonophysics 327, 225–238.

Hoogerduijn Strating, E., Rampone, E., Piccardo, G.B., Drury, M.R., Vissers, R.L.M., 1993. Subsolidus emplacement of mantle peridotites during incipient oceanic rifting and opening of the Mesozoic Tethys (Voltri Massif, NW Italy). J. Petrol. 34 (5), 901–927.

Hua, Y., Zhao, D., Xu, Y., 2017. P-wave anisotropic tomography of the Alps. J. Geophys. Res. 122, 4509–4528.

Jolivet, L., Faccenna, C., 2000. Mediterranean extension and the Africa-Eurasia collision. Tectonics 19, 1095–1106.

Jolivet, L., Faccenna, C., Piromallo, C., 2009. From mantle to crust: stretching the Mediterranean. Earth Planet. Sci. Lett. 285 (1-2), 198–209.

Kissling, E., Schmid, S.M., Lippitsch, R., Ansorge, J., Fügenschuh, B., 2006. Lithosphere structure and tectonic evolution of the Alpine arc: new evidence from high-resolution teleseismic tomography. Geol. Soc. Lond. Mem. 32 (1), 129–145.

Lardeaux, J.M., Schwartz, S., Tricart, P., Paul, A., Guillot, S., Béthoux, N., Masson, F., 2006. A crustal-scale cross-section of the south-western Alps combining geophysical and geological imagery. Terra Nova 18, 412–422.

Lemoine, M., Bas, T., Arnaud-Vanneau, A., Arnaud, H., Dumont, T., Gidon, M., Bourdon, M., de Graciansky, P.C., Rudkiewicz, J.L., Megard-Galli, J., Tricart, P., 1986. The continental margin of the Mesozoic Tethys in the Western Alps. Mar. Pet. Geol. 3, 179–199.

Liao, J., Gerya, T., Malusà, M.G., 2018. 3D modeling of crustal shortening influenced by along-strike lithological changes: Implications for continental collision in the Western and Central Alps. Tectonophy. http://dx.doi.org/10.1016/j.tecto.2018.01.031. (in press).

Lippitsch, R., Kissling, E., Ansorge, J., 2003. Upper mantle structure beneath the Alpine orogen from high-resolution teleseismic tomography. J. Geophys. Res. 108 (B8).

Long, M.D., Becker, T.W., 2010. Mantle dynamics and seismic anisotropy. Earth Planet. Sci. Lett. 297, 341–354.

Long, M.D., Silver, P.G., 2008. The subduction zone flow field from seismic anisotropy: a global view. Science 319 (5861), 315–318.

Long, M.D., Silver, P.G., 2009. Shear wave splitting and mantle anisotropy: measurements, interpretations, and new directions. Surv. Geophys. 30, 407–461.

Long, M.D., Till, C.B., Druken, K.A., Carlson, R.W., Wagner, L.S., Fouch, M.J., ... Kincaid, C., 2012. Mantle dynamics beneath the Pacific Northwest and the generation of voluminous back-arc volcanism. Geochem. Geophys. Geosyst. 13 (8).

Lucente, F.P., Chiarabba, C., Cimini, G.B., Giardini, D., 1999. Tomographic constraints on the geodynamic evolution of the Italian region. J. Geophys. Res. 104, 20,307–20,327.

Lucente, F.P., Margheriti, L., Piromallo, C., Barruol, G., 2006. Seismic anisotropy reveals the long route of the slab through the western-central Mediterranean mantle. Earth Planet. Sci. Lett. 241, 517–529.

Lyu, C., Pedersen, H.E., Paul, A., Zhao, L., Solarino, S., the CIFALPS Working Group, 2017. Shear wave velocities in the upper mantle of the Western Alps: new constraints using array analysis of seismic surface waves. Geophys. Res. Lett. 210, 321–331.

Mainprice, D., Barruol, G., Ismail, W.B., 2000. The seismic anisotropy of the Earth's mantle: from single crystal to polycrystal. In: Earth's Deep Interior: Mineral Physics and Tomography From the Atomic to the Global Scale, pp. 237–264.

Malusà, M.G., Anfinson, O.A., Dafov, L.N., Stockli, D.F., 2016a. Tracking Adria indentation beneath the Alps by detrital zircon U-Pb geochronology: implications for the Oligocene–Miocene dynamics of the Adriatic microplate. Geology 44, 155–158.

Malusà, M.G., Danišík, M., Kuhlemann, J., 2016b. Tracking the Adriatic-slab travel beneath the Tethyan margin of Corsica-Sardinia by low-temperature thermochronometry. Gondwana Res. 31, 135–149.

Malusà, M.G., Balestrieri, M.L., 2012. Burial and exhumation across the Alps-Apennines

junction zone constrained by fission-track analysis on modern river sands. Terra Nova 24, 221–226.

Malusà, M.G., Faccenna, C., Baldwin, S.L., Fitzgerald, P.G., Rossetti, F., Balestrieri, M.L., Danišík, M., Ellero, A., Ottria, G., Piromallo, C., 2015. Contrasting styles of (U)HP rock exhumation along the Cenozoic Adria-Europe plate boundary (Western Alps, Calabria, Corsica). Geochem. Geophys. Geosyst. 16, 1786–1824.

Malusà, M.G., Zhao, L., Eva, E., Solarino, S., Paul, A., Guillot, S., Schwartz, S., Dumont, T., Aubert, C., Salimbeni, S., Pondrelli, S., Wang, Q., Zhu, R., 2017. Earthquakes in the western alpine mantle wedge. Gondwana Res. 44, 89–95.

Manatschal, G., 2004. New models for evolution of magma-poor rifted margins based on a review of data and concepts from West Iberia and the Alps. Int. J. Earth Sci. 93 (3), 432–466.

Manatschal, G., Müntener, O., 2009. A type sequence across an ancient magma-poor ocean–continent transition: the example of the western Alpine Tethys ophiolites. Tectonophy 473, 4–19.

Margheriti, L., Lucente, F.P., Pondrelli, S., 2003. SKS splitting measurements in the Apenninic-Tyrrhenian domain (Italy) and their relation with lithospheric subduction and mantle convection. J. Geophys. Res. 108, 2218 B4.

Marty, B., O'Nions, R.K., Oxburgh, E.R., Martel, D., Lombardi, S., 1992. Helium isotopes in Alpines regions. Tectonophysics 206, 71–78.

Mercier, J.P., Bostock, M.G., Audet, P., Gaherty, J.B., Garnero, E.J., Revenaugh, J., 2008. The teleseismic signature of fossil subduction: northwestern Canada. J. Geophys. Res. Solid Earth 113 (B4).

Nguyen, H.N., Vernant, P., Mazzotti, S., Khazaradze, G., Asensio, E., 2016. 3-D GPS velocity field and its implications on the present-day post-orogenic deformation of the Western Alps and Pyrenees. Solid Earth 7 (5), 1349–1363.

Nicolas, A., Bouchez, J.L., Boudier, F., 1972. Interprétation cinématique des déformations plastiques dans le massif de lherzolite de Lanzo (Alpes piemontaises) - comparaison avec d'autres massifs. Tectonophysics 14 (2), 143–171.

Nocquet, J.M., Sue, C., Walpersdorf, A., Tran, T., Lenôtre, N., Vernant, P., Cushing, M., Jouanne, F., Masson, F., Baize, S., Chéry, J., van der Beek, P.A., 2016. Present-day uplift of the western Alps. Sci. Rep. 6, 28404.

Pearce, J., Mittleman, D., 2002. Defining the Fresnel zone for broadband radiation. Phys. Rev. E 66, 056602.

Piccardo, G.B., Vissers, R.L.M., 2007. The pre-oceanic evolution of the Erro-Tobbio peridotite (Voltri Massif, Ligurian Alps, Italy). J. Geodyn. 43 (4), 417–449.

Piromallo, C., Becker, T.W., Funiciello, F., Faccenna, C., 2006. Three-dimensional instantaneous mantle flow induced by subduction. Geophys. Res. Lett. 33 (8).

Piromallo, C., Morelli, A., 2003. P wave tomography of the mantle under the Alpine–Mediterranean area. J. Geophys. Res. 108 (B2).

Qorbani, E., Bianchi, I., Bokelmann, G., 2015. Slab detachment under the Eastern Alps seen by seismic anisotropy. Earth Planet. Sci. Lett. 409, 96–108.

Salimbeni, S., Pondrelli, S., Margheriti, L., 2013. Hints on the deformation penetration induced by subductions and collision processes: seismic anisotropy beneath the Adria region (Central Mediterranean). J. Geophys. Res. 118, 5814–5826.

Salimbeni, S., Pondrelli, S., Margheriti, L., Park, J., Levin, V., 2008. SKS splitting measurements beneath Northern Apennines region: a case of oblique trench retreat. Tectonophysics 462, 68–82.

Savage, M.K., 1999. Seismic anisotropy and mantle deformation: what have we learned from shear wave splitting? Rev. Geophys. 37, 65–106.

Savage, M.K., Sheehan, A.F., 2000. Seismic anisotropy and mantle flow from the Great Basin to the Great Plains, western United States. J. Geophys. Res. 105, 13,715–13,734.

Scambelluri, M., Müntener, O., Hermann, J., Piccardo, G.B., Trommsdorff, V., 1995. Subduction of water into the mantle: history of an Alpine peridotite. Geology 23 (5), 459–462.

Schellart, W.P., 2004. Kinematics of subduction and subduction-induced flow in the upper mantle. J. Geophys. Res. Solid Earth 109 (B7).

Schellart, W.P., 2010. Mount Etna–Iblean volcanism caused by rollback-induced upper mantle upwelling around the Ionian slab edge: an alternative to the plume model. Geology 38 (8), 691–694.

Selverstone, J., 2005. Are the Alps collapsing? Annu. Rev. Earth Planet. Sci. 33, 113–132.

Serpelloni, E., Faccenna, C., Spada, G., Dong, D., Williams, S.D., 2013. Vertical GPS ground motion rates in the Euro-Mediterranean region: new evidence of velocity gradients at different spatial scales along the Nubia-Eurasia plate boundary. J. Geophys. Res. 118, 6003–6024.

Shinohara, M., Fukano, T., Kanazawa, T., Araki, E., Suyehiro, K., Mochizuki, M., Nakahigashi, K., Yamada, T., Mochizuki, K., 2008. Upper mantle and crustal seismic structure beneath the Northwestern Pacific Basin using a seafloor borehole broad-band seismometer and ocean bottom seismometers. Phys. Earth Planet. Inter. 170 (1), 95–106.

Silver, P.G., Chan, W.W., 1991. Shear wave splitting and subcontinental mantle deformation. J. Geophys. Res. 96, 16,429–16,454.

Silver, P.G., Mainprice, D., Ismail, W.B., Tommasi, A., Barruol, G., 1999. Mantle structural geology from seismic anisotropy. Spec. Publ. Geochem. Soc. 6, 79–103.

Solarino, S., Malusà, M.G., Eva, E., Guillot, S., Paul, A., Schwartz, S., Zhao, L., Aubert, C., Dumont, T., Pondrelli, S., Salimbeni, S., Wang, Q., Xu, X., Zheng, T., Zhu, R., 2018. Mantle wedge exhumation beneath the Dora-Maira (U)HP dome unravelled by local earthquake tomography (Western Alps). Lithos 296–299, 623–636.

Sue, C., Thouvenot, F., Fréchet, J., Tricart, P., 1999. Widespread extension in the core of the western Alps revealed by earthquake analysis. J. Geophys. Res. 104, 25611–25622.

Tommasi, A., Tikoff, B., Vauchez, A., 1999. Upper mantle tectonics: three-dimensional deformation, olivine crystallographic fabrics and seismic properties. Earth Planet. Sci. Lett. 168 (1), 173–186.

Vauchez, A., Tommasi, A., Mainprice, D., 2012. Faults (shear zones) in the Earth's mantle.

Tectonophysics 558, 1–27.

Vignaroli, G., Faccenna, C., Jolivet, L., Piromallo, C., Rossetti, F., 2008. Subduction polarity reversal at the junction between the Western Alps and the Northern Apennines, Italy. Tectonophysics 450, 34–50.

Vissers, R.L.M., Drury, M.R., Hoogerduijn Strating, E., Spiers, C.J., Van der Wal, D., 1995. Mantle shear zones and their effect on lithosphere strength during continental breakup. Tectonophysics 249 (3–4), 155–171.

Walpersdorf, A., Sue, C., Baize, S., Cotte, N., Bascou, P., et al., 2015. Coherence between geodetic and seismic deformation in a context of slow tectonic activity (SW Alps, France). J. Geodyn. 85, 58–65.

Winterer, E.L., Bosellini, A., 1981. Subsidence and sedimentation on Jurassic passive continental margin, Southern Alps, Italy. AAPG Bull. 65 (3), 394–421.

Wittmann, H., Malusà, M.G., Resentini, A., Garzanti, E., Niedermann, S., 2016. The cosmogenic record of mountain erosion transmitted across a foreland basin: source-to-sink analysis of in situ ^{10}Be, ^{26}Al and ^{21}Ne in sediment of the Po river catchment. Earth Planet. Sci. Lett. 452, 258–271.

Wüstefeld, A., Bokelmann, G., 2007. Null detection in shear-wave splitting

measurements. Bull. Seismol. Soc. Am. 97 (4), 1204–1211.

Wüstefeld, A., Bokelmann, G., Zaroli, C., Barruol, G., 2008. SplitLab: a shear-wave splitting environment in Matlab. Comput. Geosci. 34, 515–528.

Zandt, G., Humphreys, E., 2008. Toroidal mantle flow through the western US slab window. Geology 36 (4), 295–298.

Zhao, L., Paul, A., Guillot, S., Solarino, S., Malusà, M.G., Zheng, T., Aubert, C., Salimbeni, S., Dumont, T., Schwartz, S., Zhu, R., Wang, Q., 2015. First seismic evidence for continental subduction beneath the Western Alps. Geology 43, 815–818.

Zhao, L., Paul, A., Malusà, M.G., Xu, X., Zheng, T., Solarino, S., Guillot, S., Schwartz, S., Dumont, T., Salimbeni, S., Aubert, C., Pondrelli, S., Wang, Q., Zhu, R., 2016. Continuity of the Alpine slab unraveled by high-resolution *P*-wave tomography. J. Geophys. Res. http://dx.doi.org/10.1002/2016JB013310.

Zhao, L., Paul, A., Solarino, S., 2016. Seismic Network YP: CIFALPS Temporary Experiment (China-Italy-France Alps Seismic Transect). RESIF - Réseau Sismologique et Géodésique Français. Seismic Network http://dx.doi.org/10.15778/RESIF.YP2012.

Zhu, H., Tromp, J., 2013. Mapping tectonic deformation in the crust and upper mantle beneath Europe and the North Atlantic Ocean. Science 341, 871–875.